MRS Communications (2015), 5, 77–82

doi:10.1557/mrc.2014.37

MRS Communications

Research Letters

Indentation-induced two-way shape-memory effect in aged Ti-50.9 at.% Ni

Mareike Frensemeier and **Eduard Arzt,** INM—Leibniz Institute for New Materials, Saarbrücken 66123, Germany; Saarland University, Saarbrücken 66123, Germany
Enwei Qin, Suzhou Nuclear Power Research Institute Co., Ltd., Suzhou 215004, China
Carl P. Frick, Department of Mechanical Engineering, University of Wyoming, Laramie, Wyoming 82071
Andreas S. Schneider†, INM—Leibniz Institute for New Materials, Saarbrücken 66123, Germany

Address all correspondence to Mareike Frensemeier at **mareike.frensemeier@inm-gmbh.de**

(Received 25 September 2014; accepted 11 December 2014)

Abstract

In this study, Vickers indentation was used to investigate the two-way shape-memory effect (TWSME) in an austenitic Ti-50.9 at.% Ni alloy, exposed to different heat treatments. Three aging treatments were used to manipulate the size of Ti_3Ni_4 precipitates. All samples were Vickers indented, and the indent depth was investigated as function of thermal cycling. The TWSME was found only in the material aged at 400 °C, which contained coherent precipitates. Thermal cycling shows stable TWSME, however, heating well above the austenite finish temperature lead to permanent austenitic protrusions. The results indicate that stabilized martensite plays a critical role in creating TWSME surfaces.

Introduction

Nickel–titanium (NiTi) shape-memory alloys are capable of recovering their previously defined shape after certain deformation upon the application of heat. This recovery, called one-way shape memory effect (OWSME), is due to a stress-induced martensitic phase transformation, i.e., a coordinated shift in atomic structure that is completely reversible even for large strains up to approximately 8–12%.[1] Through an appropriate combination of deformation processing and/or heat treatment, it is possible to elicit a switchable TWSME.[2] This effect is characterized by the alloy's memorization of the high- and low-temperature shape, allowing for spontaneous change between these shapes as a function of cycling temperature. The intrinsic mechanism that dictates the TWSME remains a subject of research interest.

Recent studies have shown that a TWSME surface can be induced in NiTi using an indentation method.[3–5] The near equiatomic NiTi samples were indented to high strains, thermally cycled, then planarized, and re-polished. When the sample was reheated into the austenite phase, protrusions formed on the sample surface, a phenomenon found to be repeatable over multiple heating cycles. The protrusions were hypothesized to be caused by preferentially oriented dislocation structures, which remained underneath and around the indentation site after planarization. A more recent microstructural characterization performed on Ti-50.9 at.% Ni shape-memory surfaces after Vickers indentation revealed both dislocations and thermally stabilized martensitic plates parallel to the indents.[6] It was theorized that this stabilized martensite may act as nucleation seed for the TWSME. However, more detailed testing is necessary for a deeper understanding of these TWSME surfaces.

The purpose of this study is to expand the limited experimental studies on TWSME surfaces by investigating the effect of pre-existing Ti_3Ni_4 precipitates. For slightly Ni-rich NiTi, precipitates are well known to influence the martensitic phase transformation. It has been shown that coherent Ti_3Ni_4 precipitates increase the stress necessary for plastic flow and decrease the martensite transformation stress (e.g., [7,8]). Essentially, local stress fields caused by precipitates act in addition to an applied external stress, and become the location of the phase transformation. Thus, the transformation stress scales inversely with the precipitate coherency. Unfortunately, the role of pre-existing precipitates on the indentation-induced TWSME is not well understood. Therefore our approach was to vary the aging time systematically, leading to either: (i) solutionized, (ii) coherent, or (iii) incoherent Ti_3Ni_4 precipitates. TWSME surfaces were then created via Vickers indentation followed by planarization. The results show that coherent precipitates were critical for good TWSME behavior and the protrusion height as well as the two-way deformation recovery were sensitive to the re-heat temperature. The observed behavior is discussed in terms of the underlying microstructural mechanisms.

Experimental

Three bulk samples were electro-discharge machined from rod stock of a cold-drawn Ti-50.9 at.% Ni alloy, used in previous studies.[6,9] These samples were oven heated to 700 °C for

† Current address: AG der Dillinger Hüttenwerke, Dillingen, Germany.

Table I. Transformation temperatures derived from DSC curves for the tested NiTi materials (A, austenite; M, martensite; R, R-phase).

[f]Finish temperature	Heating (°C)				Cooling (°C)			
[s]Start temperature	R_s	R_f	A_s	A_f	R_s	R_f	M_s	M_f
Solutionized	–	–	−13	−3	–	–	−28	−43
400 °C aging	26	35	37	45	50	35	47	−20
550 °C aging	–	–	−8	4	–	–	−26	−39

1.5 h and then immediately water quenched, which is well known to lead to a solutionized microstructure. The solutionized NiTi has an austenitic B2 structure at room temperature. Two of the solutionized samples were aged for 1.5 h and water quenched at 400 and at 550 °C, respectively. These aging treatments were explicitly aimed at generating either coherent (400 °C) or incoherent precipitates (550 °C).

Using a wire-cutting saw, slices weighing approximately 10 mg were prepared for thermal analysis by differential scanning calorimetry (DSC) using a Mettler Toledo DSC1 Star System. The heating/cooling rate was set as 20 °C/min. The phase transformation temperatures were obtained by tangent methods and listed in Table I.

The microstructures of the aged specimens were investigated via a Philips CM200 transmission electron microscope (TEM). Electron transparent samples were prepared by grinding (down to 4000 grade SiC paper) discs of 3 mm diameter to a final thickness of 50 μm and subsequent twin jet polishing at 20 V using an electrolyte of 20 vol.% sulfuric acid and 80 vol.% methanol.

Deformation recovery was investigated by measuring the depth of Vickers indents, as a function of thermal cycling. Samples were grinded down to 4000 grade SiC paper, followed by electropolishing with an electrolyte solution composed of 20 vol.% sulfuric acid and 80 vol.% methanol, leading to a final average roughness (R_a) of approximately 0.15 μm. Indentation was performed with a Leco v-100 indenter at room temperature with a load of 20 N, a loading time of approximately 5 s and a holding time of 10 s. The depth of the indents was measured via white-light interferometry (Zygo NewView 5000) at room temperature, after subsequent heating above the transformation temperature, and after cooling with liquid nitrogen (ln) at room temperature. Measurements of the indent depth in the initial and heated state were taken in situ using a custom-built heating stage.

To generate the TWSME surface for the protrusion analysis an array of six Vickers indents with an interspacing of 900 μm from center to center was indented into a polished surface. A maximum load of 200 N, a loading time of approximately 5 s, and a holding time of 10 s was used. The higher load was chosen to increase the size of the protrusions, which correlates with the indentation diameter and depth. Thus, the indent diameter of approximately 300 μm leads to protrusions of approximately 300 μm in diameter. Based on preliminary analysis, the large interspace between the indents was chosen to avoid any interaction of the intrinsic stress fields induced by the indents.

The residual indents were removed via grinding and electropolishing, to a depth just below the indents as estimated optically. The re-planarized and trained surface showed reversible protrusions of several microns upon heating and re-flattening after cooling. Measurements of the protrusion height at different maximum temperatures of 80, 100, 120, 160, and 200 °C and subsequent cooling with ln in between each cycle, were carried out.

Results and discussion

The characteristic phase transformation temperatures of the three investigated materials, shown in Fig. 1 were measured by DSC. The specific transformation temperatures are listed in Table I. The solutionized material exhibits a one-step transformation from austenite to martensite, with all transformation temperatures well below room temperature. This is expected due to the excess Ni content above equiatomic.[2] Upon aging at 400 °C for 1.5 h, the transformation temperatures increase. Notably, a secondary peak appears for both heating and cooling. This is associated with an intermediate orthorhombic phase, termed the R-phase. The presence of the R-phase is typical for aged, Ni-rich, NiTi.[9,10] The specimen aged at 550 °C for 1.5 h resembles more closely the solutionized NiTi, although the phase transformation temperatures are significantly higher.

The microstructure of the two aged NiTi samples used in this study is shown in the representative bright-field TEM images in Fig. 2. The solutionized NiTi was not explicitly investigated as thermal history and DSC measurements strongly indicate that the material has been solutionized.[11] The sample aged at 400 °C [Fig. 2(a)] shows precipitates with a length of approximately 100 nm, leading to strong internal strain fields in the microstructure due to their coherency [11]. These homogenously distributed precipitates lead to intrinsic stress fields by means of austenitic lattice distortion. The strain fields assist in the stress-induced martensitic phase transformation, and effectively increase the phase transformation temperatures.[7,8,11] The primary and brightest pattern observed in the selected area diffraction pattern [Fig. 2(a)—inset] are from the $[\overline{1}11]$ B2 zone axis confirming the presence of austenite. The secondary, weak

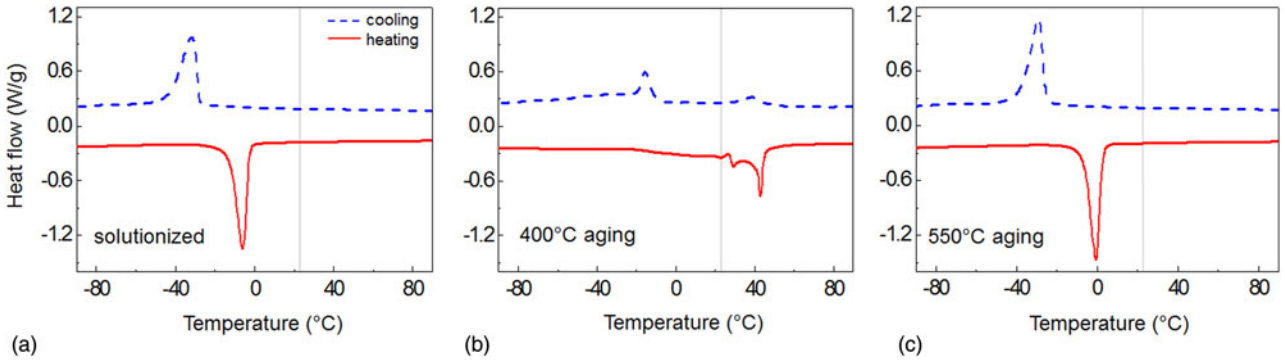

Figure 1. Representative DSC curves for the three tested NiTi samples: (a) solutionized, (b) solutionized then aged at 400 °C for 1.5 h, (c) solutionized then aged at 550 °C for 1.5 h. The dashed line indicates cooling and the vertical line represents room temperature, where all indentation testing was performed.

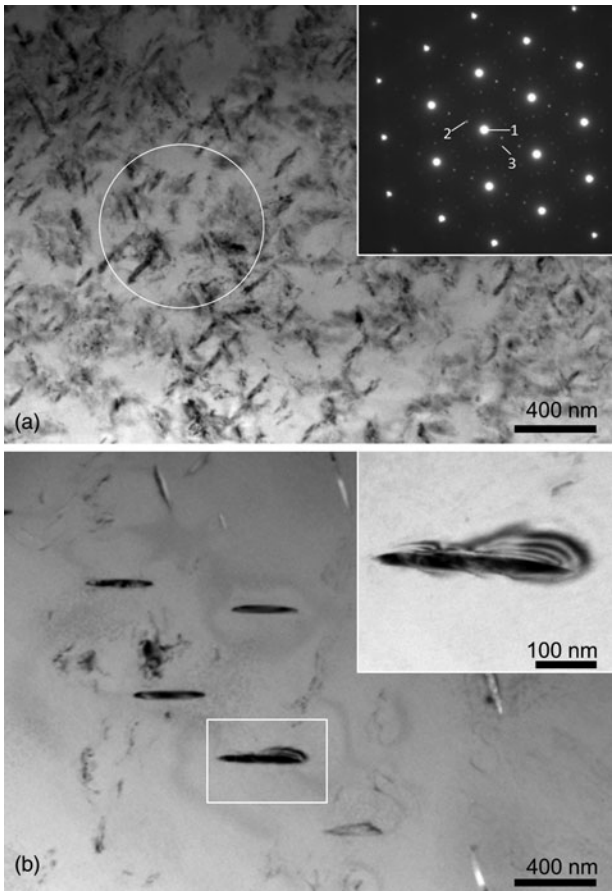

Figure 2. Bright-field TEM images of NiTi aged at (a) 400 °C and (b) 550 °C. Both heat treatments lead to lenticular-shaped Ti_3Ni_4 precipitates. The diffraction pattern [(a), inset, aperture 800 nm] shows mainly austenitic phase (1, [$\bar{1}11$] B2) with weak reflections at the 1/3 [110] B2 positions, revealing the presence of the R-phase (2) and Ti_3Ni_4 precipitates lying at 1/7 [321] B2 (3). Further heat treatment shows increasing precipitation size with stress-induced fringe contrast [(b), inset].

reflections stem from the R-phase at 1/3 [110] B2 positions, and from the Ti_3Ni_4 precipitates lying at 1/7 [321] B2 positions. The DSC curves [Fig. 1] are consistent with the assumption of the presence of the R-phase; however, it is clear that the 400 °C aged material is mostly austenite. TEM images of the 550 °C aged specimen [Fig. 2(b)] show that the lenticular Ti_3Ni_4 precipitates have increased in size to several hundred nanometers. The inset in Fig. 2(b) illustrates a stress induced fringe contrast in proximity to a precipitate. Nonetheless, the 550 °C aged specimens show a lower overall internal distortion compared with the 400 °C aging, which is consistent with overaging. Thus, the microstructural features of the different samples have to be considered as a fully austenitic lattice for the solutionized material, high amount of intrinsic stress fields induced by coherent precipitates of mid-size precipitates for the 400 °C aged material, and overaged precipitates leading into semi/non-coherent interface to the austenitic phase for the 550 °C aged material.

Each of the three samples was deformed via Vickers indentation with a load of 20 N, which was performed at room temperature. The indent depth was quantified in the heated and the cooled states by white-light interferometry, as tabulated in Table II. Previous studies have shown that the TWSME effect can be directly observed by measuring repeated indentation depth recovery.[3–6] The results show depths taken immediately after indentation, after first heating to 80 °C, after cooling with ln, then after reheating to 80 °C. The OWSME recovery ratio (RR_{OW}) and TWSME recovery ratio (RR_{TW}) can be calculated using the respective changes in indentation depth.[11–13] For the OWSME the recovery ratio is defined as:

$$RR_{OW} = (d_i - d_h)/d_i \quad (1)$$

and for the TWSME it is:

$$RR_{TW} = (d_c - d_h)/d_c, \quad (2)$$

where d_i is the initial depth, d_h is the depth after heating above A_f (austenite finish temperature), and d_c is the depth after cooling below M_f (martensite finish temperature).

Table II. White-light interferometry measurements of indentation depths. All measurements were taken at room temperature, prior to either heating above 80 °C or prior to cooling with liquid nitrogen.

	One-way shape-memory effect				Two-way shape-memory effect			
	Initial indent (μm)	After 1st heating (μm)	Recovery (μm)	Recovery ratio (%)	Repeated cooling (μm)	Repeated heating (μm)	Recovery (μm)	Recovery ratio (%)
Solutionized	12.0	10.3	1.7	14.0	9.0	9.0	0.0	0.0
400 °C aging	15.5	9.1	6.4	41.0	10.0	9.1	0.9	9.0
550 °C aging	12.0	11.0	1.0	8.0	9.0	9.0	0.0	0.0

The results in Table II illustrate that all three materials show some permanent deformation and some indent recovery upon the first heating (i.e., the OWSME). Therefore, a combination of martensite and plasticity must exist in the deformed material beneath the residual indent. The solutionized and 550 °C aged samples exhibit similar RR_{OW} values of 14 and 8%, respectively. The 400 °C aged sample exhibits a larger RR_{OW} of 41%. Similar values have been reported in literature[11,13] and can be best understood by considering the Clausius–Clapeyron relationship.[14] For conventional uniaxial testing, deformation at temperatures below A_s leads to shape-memory and above A_f to pseudoelastic behavior. With increasing strain beyond what can be accommodated by martensitic phase transformation and reorientation, plasticity of the martensite is expected. As Vickers indentation leads to a complex three-dimensional (3D) stress-state, with a strong spatial strain gradient beneath the indent, it is not as straightforward to characterize; however, the same basic relationship holds true. For the solutionized and 550 °C aged materials, indentation at room temperature is well-above A_f, and therefore a significant fraction of the phase transformation deformation is expected to be pseudoelastic (i.e., will spontaneously recover upon unloading). The presence of any RR_{OW} is an indication that martensite is stabilized due to deformation beneath the indent, even though the testing temperature is well above A_f. Several studies have shown stabilized martensite due to plastic deformation (e.g., [15–19]). It is theorized that additional heating is required to overcome a frictional effect associated with residual plasticity which prevents the deformation stabilized martensite from fully returning to austenite. For the 400 °C aged material, the volume of deformation stabilized martensite is expected to be much larger, subsequently a larger shape-memory effect and RR_{OW} is found.

With additional heating and cooling cycles the reversible TWSME was only observed in the 400 °C aged sample; thus, only this material was used for the analysis of TWSME surfaces. To create TWSME surface protrusions, the sample was deformed with an array of six Vickers indents at a load

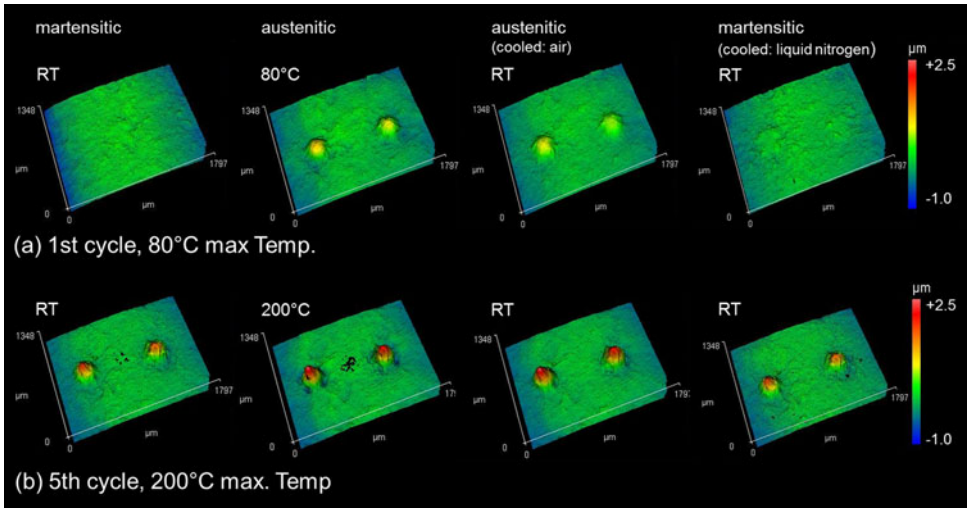

Figure 3. 3D Surface topography changes during subsequent temperature cycles taken via white-light-interferometry with 80, 100, 120, 160, 200 °C maximum temperature. Representative results are shown for the initial cycle with 80 °C maximum and the last cycle with 200 °C maximum temperature. A high ratio of the TWSME recovery is shown at maximum temperature of 80 °C, (a), and almost no TWSME remains after reaching the upper "transformation-temperature-threshold", in this case 200 °C (b).

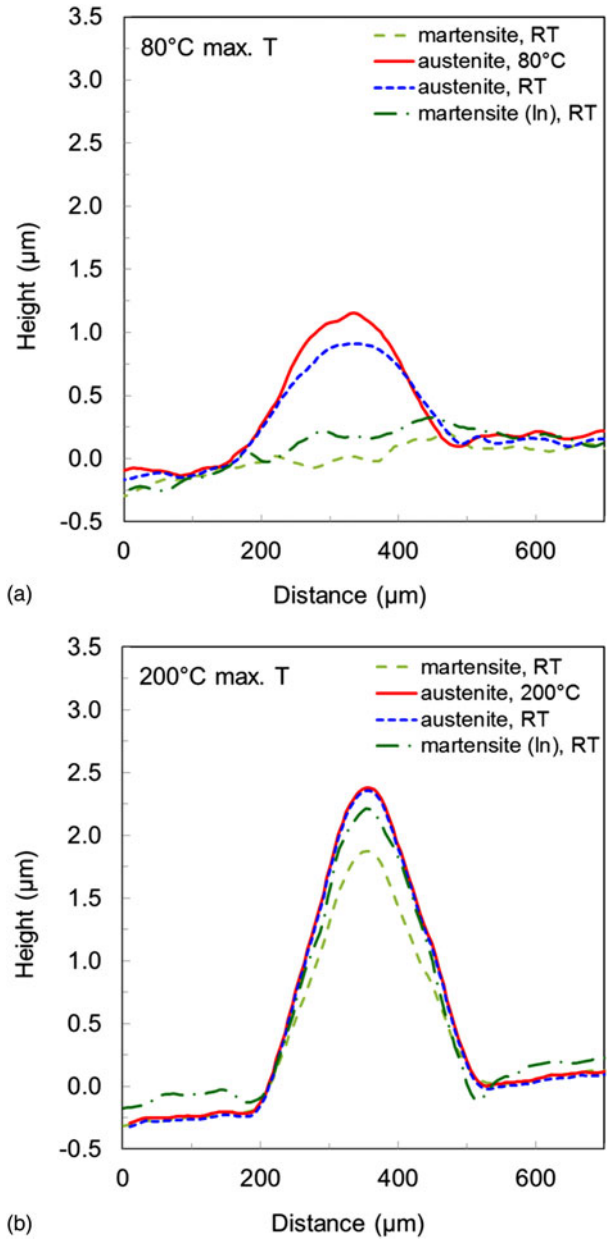

Figure 4. Cross-section profiles of surface protrusions after different temperature cycles. Shown are profiles of the initial martensitic state, after heating (austenitic state), after subsequent cooling in air to room temperature (austenitic state) and again after cooling with liquid nitrogen (martensitic state). (a) High reversibility is shown for lower maximum temperatures like 80 °C. (b) Increasing protrusion height is shown for higher maximum temperatures such as 200 °C. Low reversibility and remaining TWSME is shown by second cycling with 200 °C max. temperature.

of 200 N. Afterwards the deformed surface was ground and re-planarized. An interferometer was used to quantify this TWSME surface as a function of thermally cycling between ln and progressively increasing temperatures of 80, 100, 120, 160, and 200 °C. The temperature-dependent shape recovery behavior for two representative protrusions is shown in

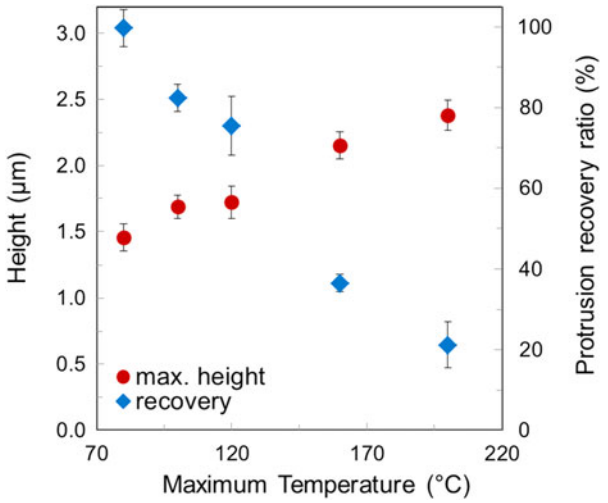

Figure 5. Comparison of protrusion height and recovery ratio during thermal cycling. Within increasing maximum cycle temperature, protrusion height steadily increases, while the TWSME decreases.

Fig. 3. For example, only the first cycle where the sample is exposed to a maximum temperature of 80 °C (top row) and the progressively last cycle with 200 °C (bottom row) maximum temperature are shown. For the first cycle the replanarized flat sample was heated up to 80 °C, and protrusions arise after exceeding the transformation temperature. They reach approximately 1.3 µm in height and exhibit reversible TWSME behavior (Fig. 4). They remain stable when allowed to cool in air to room temperature and disappear after cooling with ln. This phenomenon was observed to be repeatable over ten cycles. After being exposed to progressively increasing thermal cycles with a maximum temperature of 200 °C, the same protrusions become stable upon temperature cycling and did no longer illustrate the TWSME (Fig. 3, bottom row). Owing to this no flat surface is regained after cooling with lN. Furthermore, the protrusion height in the high-temperature state at 200 °C increased to approximately 2.4 µm. The progression of the protrusion height and the protrusion height recovery as a function of the thermal cycling is summarized in Fig. 5. It is observed that the increase in height and decrease in recovery scales with the maximum temperature until the TWSME is virtually no longer present.

To interpret the results, shown in Figs. 4 and 5 studies, which have investigated the TWSME have to be considered. The TWSME can be induced via preferential orientation of precipitates or thermo-mechanical training over several cycles, neither of which has been performed in this study. It can also be induced by severe plastic deformation of martensite. For indentation-induced TWSME surfaces, the underlying mechanism has been hypothesized to be dislocation arrays beneath the indent which lead to preferential martensite orientation.[3–5] This hypothesis has been supported by recent TEM observations of patterns formed in NiTi via laser shock-assisted direct

imprinting,[20] where a significant increase in the dislocation density is shown. However, current investigations have shown both dislocations and stabilized martensite beneath residual indents, even after thermal cycling from room temperature to 120 °C.[6] Dislocation-induced stabilized martensite has also been observed in previous work.[15–18] For the TWSME surfaces, it was theorized that the stabilized martensite acts as a nucleation point for the phase transformation, which is supported by the results shown in Fig. 3. Although cycling progressively from 80 to 200 °C is not sufficient to cause significant dislocation annihilation or precipitate growth, it would be appropriate for overcoming internal friction due to dislocations structures and transforming the stabilized martensite back to austenite. Also, it is important to note that the height of the protrusions becomes larger with increasing cycle temperature (Fig. 5), which is consistent with dislocation-stabilized martensite returning back to austenite. Consequently, it remains our belief that the stabilized martensite plays a critical role in indentation-induced TWSME surfaces.

In comparison to the present work, previous investigations on TWSME surfaces have been carried out exclusively on Ti-50.3 at.% Ni material, where only martensite is stable at room temperature. It is therefore possible that the combination of testing temperature and composition may lead to different mechanisms which dictate the TWSME surfaces. Systematic investigation into the effect of composition and indentation temperature is currently underway.

Conclusions

In summary, indentation-induced TWSME is only shown in the material, which was solutionized and subsequently aged at 400 °C, containing semi-coherent Ti_3Ni_4 precipitates with a size of about 100 nm. The indentation-induced stress fields contribute to the activation of corresponding martensite variants. Within thermal cycling up to moderate temperatures no tendency of fatigue was shown, the surface protrusions are highly reversible. Stepwise thermal cycling high above the transformation temperature leads to an increase of the protrusion's heights and simultaneously to a decrease and elimination in their reversibility. Thus, the TWSME disappears at high temperatures, which lead to the assumption that stabilized martensite is critical to generate TWSME surfaces from aged Ti-50.9 at.% Ni.

Acknowledgments

The research leading to these results has received funding from the European Research Council under the European Union's Seventh Framework Program (FP/2007-2013)/ERC Grant Agreement no. 340929. CPF gratefully acknowledges support of this work from the National Science Foundation (NSF) CAREER award (grant no. DMR-1255603), as well as the University of Wyoming International Travel Grant.

References

1. J.A. Shaw and S. Kyriakides: Thermomechanical aspects of NiTi. *J. Mech. Phys. Solids* **43**, 1243–1281 (1995).
2. K. Otsuka and X. Ren: Physical metallurgy of Ti-Ni-based shape memory alloys. *Prog. Mater. Sci.* **50**, 511–678 (2005).
3. Y.J. Zhang, Y.T. Cheng, and D.S. Grummon: Shape memory surfaces. *Appl. Phys. Lett.* **89**, 041912 (2006).
4. Y.J. Zhang, Y.T. Cheng, and D.S. Grummon: Understanding indentation-induced two-way shape memory effect. *J. Mater. Res.* **22**, 2851–2855 (2007).
5. X.L. Fei, Y.J. Zhang, D.S. Grummon, and Y.T. Cheng: Indentation-induced two-way shape memory surfaces. *J. Mater. Res.* **24**, 823–830 (2009).
6. E. Qin, N.J. Peter, M. Frensemeier, C.P. Frick, E. Arzt, and A.S. Schneider: Vickers indentation induced one-way and two-way shape memory effect in austenitic NiTi. *Adv. Eng. Mater.* **16**, 72–79 (2014).
7. K. Gall, H. Sehitoglu, Y.I. Chumlyakov, I.V. Kireeva, and H.J. Maier: The influence of aging on critical transformation stress levels and martensite start temperatures in NiTi: part II—discussion of experimental results. *J. Eng. Mater.* **121**, 28–37 (1999).
8. K. Gall, H. Sehitoglu, Y.I. Chumlyakov, I.V. Kireeva, and H.J. Maier: The influence of aging on critical transformation stress levels and martensite start temperatures in NiTi: part I—aged microstructure and micro-mechanical modeling. *J. Eng. Mater.* **121**, 19–27 (1999).
9. Y.N. Liu, H. Yang, and A. Voigt: Thermal analysis of the effect of aging on the transformation behaviour of Ti-50.9 at. % Ni. *Mater. Sci. Eng. A* **360**, 350–355 (2003).
10. J. Khalil-Allafi, A. Dlouhy, and G. Eggeler: Ni4Ti3-precipitation during aging of NiTi shape memory alloys and its influence on martensitic phase transformations. *Acta Mater.* **50**, 4255–4274 (2002).
11. C.P. Frick, A.M. Ortega, J. Tyber, A.E.M. Maksound, H.J. Maier, Y.N. Liu, and K. Gall: Thermal processing of polycrystalline NiTi shape memory alloys. *Mater. Sci. Eng. A* **405**, 34–49 (2005).
12. W.Y. Ni, Y.T. Cheng, and D.S. Grummon: Recovery of microindents in a nickel–titanium shape-memory alloy: a "self-healing" effect. *Appl. Phys. Lett.* **80**, 3310–3312 (2002).
13. G.A. Shaw, D.S. Stone, A.D. Johnson, A.B. Ellis, and W.C. Crone: Shape memory effect in nanoindentation of nickel–titanium thin films. *Appl. Phys. Lett.* **83**, 257–259 (2003).
14. K. Otsuka and C.M. Wayman: *Shape Memory Materials* (Cambridge University Press, Cambridge, UK, 1998).
15. H.C. Lin, S.K. Wu, T.S. Chou, and H.P. Kao: The effects of cold-rolling on the martensitic-transformation of an equiatomic tini alloy. *Acta Metall. Mater.* **39**, 2069–2080 (1991).
16. Y.N. Liu and D. Favier: Stabilisation of martensite due to shear deformation via variant reorientation in polycrystalline NiTi. *Acta Mater.* **48**, 3489–3499 (2000).
17. A.S. Mahmud, H. Yang, S. Tee, G. Rio, and Y. Liu: Effect of annealing on deformation-induced martensite stabilisation of NiTi. *Intermetallics* **16**, 209–214 (2008).
18. G. Laplanche, J. Pfetzing-Micklich, and G. Eggeler: Orientation dependence of stress-induced martensite formation during nanoindentation in NiTi shape memory alloys. *Acta Mater.* **68**, 19–31 (2014).
19. J. Pfetzing, A. Schaefer, C. Somsen, and M.F.-X. Wagner: Nanoindentation of pseudoelastic NiTi shape memory alloys: thermomechanical and microstructural aspects. *Int. J. Mater. Res.* **100**, 936–942 (2009).
20. C. Ye and G.J. Cheng: Scalable patterning on shape memory alloy by laser shock assisted direct imprinting. *Appl. Surf. Sci.* **258**, 10042–10046 (2012).